NJC

ROYAL SOCIETY OF CHEMISTRY

PAPER

View Article Online
View Journal

Cite this: DOI: 10.1039/c9nj04408f

Study of the complexation of structurally modified curcumin with hydroxypropyl beta cyclodextrin and its effect on anticancer activity

Bably Khatun, [a] Pitambar Baishya,[b] Anand Ramteke[b] and T. K. Maji *[a]

Received 26th August 2019,
Accepted 2nd February 2020

DOI: 10.1039/c9nj04408f

rsc.li/njc

There is evidence that the structural modification of curcumin (CUR) into its pyrazole form (CP) and the complexation of CUR with hydroxypropyl beta cyclodextrin (HPβCD) both improve curcumin's chemical–physical properties and enhance its biological activities. However, making use of both strategies is scarce. This study aims at modifying CUR structurally with hydrazine hydrate and the complexation of the modified CUR with HPβCD, employing a simple protocol, which has not been reported so far. The physicochemical structural features of the prepared compounds have been probed through UV-visible (UV-Vis) spectroscopy, Fourier transform infrared (FTIR) spectroscopy, nuclear magnetic resonance (NMR) spectroscopy, X-ray diffractometry (XRD), differential scanning calorimetry (DSC), thermal gravimetric analysis (TGA) and scanning electron microscopy (SEM). The aqueous solubility of the products was enhanced as examined visibly and by UV-Vis spectroscopy and optical microscopy. The cytotoxicity of the samples in A549 lung cancer cell lines was assessed by MTT assay and cell counting through the trypan blue exclusion method. Negligible colony formation was observed as checked by clonogenic assay in the lung cancer cell lines. Besides being toxic to cancer cell lines, the samples were found to be non-toxic to human peripheral blood mononuclear cells (PBMCs), as revealed by MTT assay.

1 Introduction

Humans suffer from various life-threatening diseases such as cancer. Cancer is considered as the second most lethal disease responsible for about 21% annual death worldwide. Among different types of cancers, non-small-cell lung cancer is responsible for about 80% of lung cancer cases. The conventional treatment of cancer, mostly chemotherapy, often results in intense side effects due to the action of the drugs on sites other than the intended target.[1] Due to continuous efforts over the years, a number of anticancer drugs either of synthetic or natural origin have emerged to treat this disease. The biological activities of synthetic drugs, such as paclitaxel and cisplatin, have improved by complexing them with nanoparticles.[2] However, researchers today are paying more attention to plant-based products due to their various advantages over synthetic drugs. One such product is curcumin, the main component of the famous Indian spice turmeric.

Curcumin is a natural polyphenol compound that has been traditionally used by ancient people as a home remedy for various ailments. Over time, this compound has got considerable attention due to its variety of biological activities including antioxidant, anti-inflammation, antimicrobial and anticancer activities. It is reported to be an efficacious and safe compound for cancer therapy. The clinical trials have proved that a daily dose of 12 g for 3 months does not have adverse effects on humans. Despite the recognized pharmacological potential, the drawback of CUR lies in the fact that CUR lacks solubility and bioavailability due to its low absorption, rapid metabolism and rapid systemic elimination. To overcome such limitations, various strategies, such as structural modification[3] and complexation,[4] have been employed by researchers.

Curcumin pyrazole analogs are reported to improve the therapeutic profile of the natural product CUR, demonstrating the improvement of its bioactivities, such as antiangiogenic, antitumor, antimicrobial, anti-inflammatory, and growth suppressive activities, and being 30 times more potent compared to their raw counterpart. It is worth mentioning that the derivatives prepared showed considerable cell growth inhibitory activity against MCF-7, HeLa and K562 cell lines.[5]

A lot of CUR analogs have been studied so far but the nitrogen-containing heterocyclic moieties and their derivatives have historically been invaluable as a source of therapeutic agents. The pyrazole derivative is an example of such a compound having 2 N-atoms and aromatic character, which contributes multiple functionality and stereochemical complexity in a five-membered

[a] Department of Chemical Sciences, Tezpur University, Napaam, Tezpur, Assam, India. E-mail: tkm@tezu.ernet.in, bably@tezu.ernet.in
[b] Department of Molecular Biology & Biotechnology, Tezpur University, Napaam, Tezpur, Assam, India

ring structure. The pyrazole-based analogs among various others have manifested better biological activity.[6] In spite of these several advantages, the aqueous solubility of the simplest pyrazole derivative is unsatisfactory. One of the ways to overcome this problem is complexation with cyclodextrin.[7]

Cyclodextrins are cyclic oligosaccharides formed from starch degradation. They are inexpensive, human friendly and have better physical, chemical and biological properties. They have been used as pharmaceutical excipients for hydrophobic substances as solubilizing and stabilizing agents. Among the three different kinds of cyclodextrins (α, β and γ), β-CD is the most widely used because it is cheap, readily available and its cavity size is suitable for its interaction as a host with a guest molecule. The structure of β-CD comprises a hydrophobic core with a hydrophilic outer surface. Moreover, the addition of the hydroxyl propyl (HP) group to β-CD remarkably enhances its properties such as stability, solubility and oral bioavailability[8,9] while maintaining the bioactivity and diminishing tissue irritation. It is worth mentioning that the HP derivative of β-CD enhances aqueous solubility by more than 27 fold.[9]

Besides all of the abovementioned advantages, it is very important to note that the drug molecules should be protected from the environment and should be capable of diffusing to the site of action without losing their identity. Also, the drug must cross the lipophilic barrier to start its action. However, HPβCD fulfils all these criteria as the drug gets encapsulated into its cavity by non-covalent interactions, which are also known as host–guest action. Further, it was reported that the complexation with HPβCD controlled the drug release pattern.[10]

Taking all these factors into consideration, we planned to combine the strategies of both structural modification and complexation with a view to getting improved results. In this study, we have modified CUR to its pyrazole form by the refluxing method and characterized it using different analytical techniques. Additionally, we have prepared an inclusion complex of CP with HPβCD by the common coevaporation method and characterized it. The anticancer activity of the prepared samples was examined through MTT analysis, cell counting, and clonogenic assay. Further, the samples were checked for their toxicity in human lymphocyte cells.

2 Materials and methods

2.1 Materials

CUR (MW: 368.39) and glacial acetic acid were purchased from Sigma Aldrich, Germany, and Merck, India, respectively. Hydrazine hydrate (MW: 50.06) was purchased from Rankem, India. HPβCD (MW: *ca.* 1250–1480) was purchased from Alfa Aesar (Ward Hill, Massachusetts, USA). [3-(4,5-Dimethylthiazol-2-yl)-2,5-diphenyltetrazolium bromide] (MTT) (MW: 5655) was purchased from Sigma Aldrich, Germany. Epichlorohydrin was purchased from SRL, India. RPMI-1640, FBS (fetal bovine serum), DMEM, F-12K medium (Kaighn's Modification of Ham's F-12 Medium) and penicillin–streptomycin antibiotics were purchased from Hi-Media Laboratories, India. A549 lung cancer cell lines were purchased from the National Centre for Cell Science, Pune, India. Other reagents used were of analytical grade.

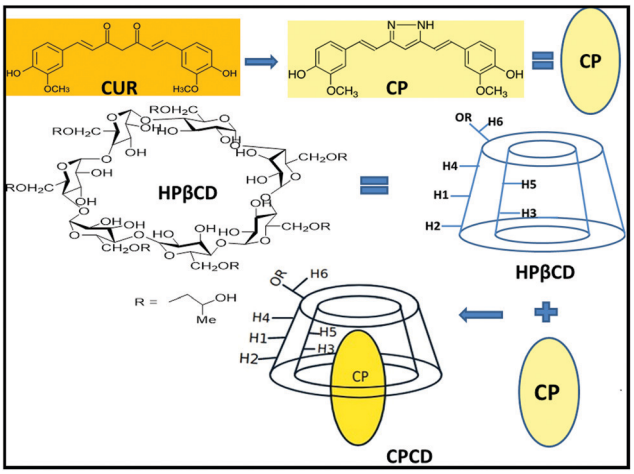

Fig. 1 Schematic diagram of the structures of CUR, CP, HPβCD and CPCD.

2.2 Synthesis of the curcumin pyrazole (CP) derivative

CP was synthesized according to the method described by Narlawar *et al.*[11] and Ahsan *et al.*[12] with minor modification. 2 g of CUR was refluxed with 660 μL of hydrazine hydrate in 20 mL of glacial acetic acid at about 60 °C for 24 h. H_2O was added to the aforementioned mixture, and the organic layer was extracted using ethyl acetate. The mixture was washed several times with water and dried over Na_2SO_4. The solvent was then evaporated, and the residue was purified by column chromatography using a mixture of ethyl acetate and hexane. It was then dried, weighed and kept at 4 °C for further analysis. The diagram showing the structures is presented in Fig. 1.

2.3 Preparation of the CP–HPβCD complex (CPCD)

The inclusion complex of CP and HPβCD was prepared by the common coevaporation technique.[13] For this, both CP and HPβCD in the ratio of 1 : 5 were separately dissolved in ethanol. Both solutions were then mixed under vigorous stirring at about 40 °C and continuously stirred till ethanol evaporated to get a fine paste. The mixture was then vacuum dried, ground to a fine powder and sieved through a 60-mesh sieve to get the final product. The sample was then weighed and kept at 4 °C for further analysis. In the literature, the molar ratio of CUR and HPβCD has been varied from 1 : 1 to 1 : 2.[7,13] In this study, the mass ratio of CP and HPβCD was kept as 1 : 5 (molar ratio: 1 : 1.35), which lies within the range available in reports. A schematic diagram of CP, HPβCD and CPCD is shown in Fig. 1.

2.4 Calculation of the process yield

The process yield of the synthesized CP and the prepared complex can be calculated by the following equations:[14]

$$\text{Process yield (\%)} = (\text{weight of CP})/(\text{weight of CUR}) \times 100$$

$$\text{Process yield (\%)} = (\text{weight of the prepared CPCD})/[\text{weight of (CP + HP}\beta\text{CD)}] \times 100.$$

2.5 Solubility study

Equal amounts of CUR, CP, HPβCD and CPCD were separately mixed with equal volumes of distilled water in four different glass vials and their solubility was checked visibly and by optical microscopy.

The aqueous solubility of the samples was further checked by UV-Vis spectrophotometry. Equal amounts of each sample were added in a specified amount of water separately in different glass vials and stirred for about half an hour. Each of the mixtures was then filtered and the filtrates were checked for their absorbance in the range 200–500 nm using a UV-Vis spectrophotometer to examine the comparative aqueous solubility of the compounds.[15]

2.6 Calibration curve of CP

A calibration curve was drawn to estimate the release rate of CP from the CPCD complex by using a 1 : 1 ethanol–water mixture. A known concentration of CP (in a 50% ethanol–water mixture) was scanned in the range 300–500 nm using a UV-Visible spectrophotometer. Peaks were observed at 336 nm for CP having a concentration in the range of 0.001–0.01 g/100 mL.[16] The absorbance values at 336 nm obtained with different concentrations of the CPCD complex were recorded and plotted. From the calibration graph (Fig. 2), the unknown concentration of CP in the CPCD complex was obtained by knowing the absorbance value.

2.7 Swelling study

Swelling studies were performed in both basic buffer (pH: 7.4) and acidic buffer (pH: 1.2) according to the procedure described in the literature.[17] 0.1 g of the prepared complex was taken in a membrane filter pouch. The empty pouch was first conditioned by immersing it in either acid or basic buffer for different time periods (0.5–24 h). The pouch containing the complex was immersed in a similar way in both acidic and basic buffers for the same time periods. The weights of the complex containing pouches after a definite time period were determined by deducting the respective conditioned weight of the empty membrane pouch. Swelling (%) was determined by measuring the change in weight of the prepared complex. The percentage of swelling for each sample determined at time 't' was calculated by the following equation:

$$\text{Swelling (\%)} = [(W_2 - W_1)/W_1] \times 100,$$

where W_1 is the initial weight of the complex before swelling, and W_2 is the final weight of the complex after swelling for a predetermined time t. The experiments were performed in triplicate and represented as a mean value.

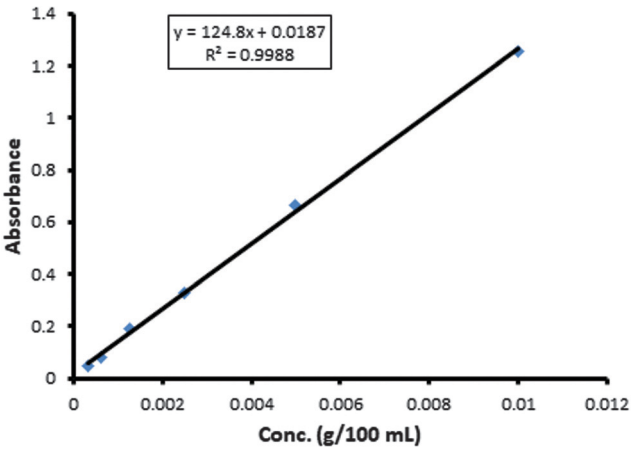

Fig. 2 Calibration curve of the curcumin pyrazole (CP) derivative.

2.8 *In vitro* drug release study

A known amount (40 mg) of the prepared complex was taken in a membrane filter pouch and immersed into a known volume (60 mL) of acidic (pH: 1.2) and basic (pH: 7.2) buffer solutions separately in two different beakers under shaking conditions for different time periods (0.5–48 h). At a scheduled time interval, 4 mL of the release medium was withdrawn, filtered and assayed at a wavelength of 336 nm using a UV-Vis spectrophotometer for the determination of the cumulative amount of drug release up to 48 h. To maintain the constant volume of the buffer solutions in the beakers, 4 mL of fresh buffer solution having the same pH was added to the respective beakers. The experiment was repeated thrice and represented as a mean value.[17]

2.9 Cell viability study

To check the cell viability of the samples in human peripheral blood mononuclear cells (PBMCs) and cancer cell lines, MTT assay was performed, and the results were analysed for lymphocyte cells and cancer cell lines after 24 h and 48 h of incubation.

2.9.1 Isolation, culture, and treatment of lymphocytes. The cytotoxic effect of the drug samples was investigated in human PBMCs. Anticoagulated human blood was collected, diluted with phosphate buffer saline (PBS) (1 : 1, v/v), layered 6 mL into 6 mL Histopaque and centrifuged at 400g for about 30 min. The lymphocytes were then separated from the buffy layer. Lymphocytes were washed by using 2 mL of PBS and 2 mL of RPMI-1640 media separately through centrifugation for 10 min at 250g.[18] After washing, the lymphocytes were further suspended in RPMI and their viability was checked by the Trypan blue exclusion method.[19] Lymphocytes having a viability of more than 90% were used for further study. 3×10^3 cells in 200 mL of isolated cells were seeded in RPMI-1640 supplemented with 10% FBS in a 96-well plate. Initially, the cells were incubated (at 37 °C in 5% CO_2) for 8 h in RPMI-1640 without FBS. The cells were then treated as per experimental requirement (MTT assay as described below) and maintained with the inclusion of FBS for 24 h.

2.9.2 Cell culture. A549 cancer cells were cultured in F-12K medium (Kaighn's Modification of Ham's F-12 Medium) containing 10% fetal bovine serum and 5% Pen–strep antibiotic solution. The cells were grown in a stable environment with 5% CO_2 at 37 °C.

2.9.3 Cytotoxicity study through MTT assay. The cytotoxicity assay was performed by measuring the viability of cells according to the method described by Denizot and Lang[20] with slight modifications. The key component [3-(4,5-dimethylthiazol-2-yl)-2,5-diphenyl tetrazolium bromide] (MTT) is yellowish in color and the mitochondrial dehydrogenase of viable cells cleaves the

tetrazolium ring, yielding purple insoluble formazan crystals.[21] This was followed by dissolving the formazan crystals in dimethyl sulphoxide (DMSO). The absorbance of the purple solution was measured spectrophotometrically. A change in the cell number resulted in a change in the amount of formazan formed, which indicated the degree of cytotoxicity caused by the material.

PBMC cells were seeded in a 96-well plate and treated with increasing concentrations of 25, 50 and 100 μg mL^{-1} of samples for a time period of 24 h at 37 °C in 5% CO_2. Similarly, A549 cells were seeded and treated with similar doses of samples for time periods of 24 h and 48 h. Cytotoxicity was determined by adding 10 μL of MTT solution (5 mg mL^{-1} in PBS) to each well, and the plate was incubated for an additional 3–4 h. The formazan crystals formed were dissolved in DMSO, and the absorbance was measured at 570–690 nm. The cell viability was determined with respect to the control cells cultured in drug-free media, and the control was considered to be 100% viable. All the experiments were repeated three times.

2.9.4 Cell counting. The cell viability was determined by the trypan blue dye exclusion method as described by Sun *et al.* with slight modifications.[22] 1×10^5 cells were seeded in a 60 mm cell culture dish and treated with 25, 50 and 100 μg mL^{-1} drug samples for 24 h at 37 °C in 5% CO_2. The cells were trypsinized and stained with trypan blue (0.4% in PBS) and counted for live/dead cells under a light microscope using a haemocytometer. All the experiments were done in triplicate.

$$\text{Viability ratio\%} = (\text{the number of viable cells})/(\text{the total number of cells}) \times 100\%.$$

2.9.5 Clonogenic assay. The assay was performed according to the previously described method by Koppikar *et al.* with slight modifications.[23] Briefly, A549 cells were plated at a seeding density of 2×10^3 cells per well in a 6-well cell culture grade plate. After 24 h, the culture medium was changed, new medium was added and the cells were exposed to various concentrations of drug samples (25, 50 and 100 μg mL^{-1}) and incubated for 24 h in 5% CO_2. Then, the treated cells were exposed to fresh media and kept in the media for 10 days for colony formation. The obtained colonies were fixed with 4% paraformaldehyde and were stained with 0.5% crystal violet solution. The colonies from the plate were counted and averaged from the observed fields randomly ($n = 3$).

The biological experiments were performed in strict accordance with the ICMR guideline, 2017, Section 11, which was approved by the Tezpur University Ethical Committee (TUEC), Memo No. DoRD/TUEC/10-14/3086-A. 2 mL of blood was collected voluntarily by the author with the help of the Institutional health centre. Informed consent was obtained from human participants of this study.

3 Statistical analysis

Statistical analysis was performed for all the biological experiments using Graph Pad Prism software, and the data were expressed as mean ± standard deviation (mean ± SD). All the results of MTT, Trypan blue exclusion and clonogenic experiments were analysed by two-way analysis of variance (ANOVA), and the differences were considered to be significant at $p < 0.05$. The significance of the samples with respect to the control (0.1% DMSO) is displayed in the respective graphs as '*a*', '*b*', '*c*' and '*n*' (p values for $a < 0.05$, $b < 0.01$, $c < 0.001$ and $n > 0.05$).

4 Characterization

4.1 UV-Vis spectrophotometry

A UV-Vis spectrophotometric technique was used for various analyses of the samples, such as structural change, solubility, drug loading and drug release profile analyses. To check whether there is any shift in the peak positions due to changes in the structure in the UV-Vis spectra, equal concentrations of CUR, CP and CPCD (0.01 g/100 mL) were taken separately in 50% ethanol–water (distilled water) mixtures and checked for their absorbance using a UV-Vis spectrophotometer (UV-2001 Hitachi, Tokyo, Japan).

4.2 Optical microscopy study

An optical microscopy study was performed to determine the compatibility of the products. For this study, aqueous dispersions of CUR, CP, HPβCD and CPCD of equivalent concentrations were prepared. A few drops of each of the dispersions were placed on separate glass slides, evenly spread and allowed to dry in a fume hood for about 20 h. The glass slides were cautiously placed to protect from dust and light. These glass slides were then placed under an optical microscope to assess the compatibility.

4.3 Fourier transform infrared (FTIR) spectroscopy

FTIR spectra of CUR, CP and the complex (CPCD) were obtained using a Nicolet (model Impact-410, USA) spectrophotometer. The nanoparticles were grounded into a powder, mixed with KBr, and the spectra were recorded in the range of 4000–400 cm^{-1}.

4.4 Nuclear magnetic resonance spectroscopy (^{1}H NMR)

The incorporation of nitrogen in place of oxygen was confirmed by proton NMR spectroscopy. Further, the interaction of CP with HPβCD to form the complex was also confirmed. The analysis was done using a 400 MHz FTNMR (Jeol, Japan) spectrophotometer.

4.5 X-ray diffractometry (XRD)

The changes in crystallinity in CP and CPCD were examined by X-ray diffractometry. XRD was carried out using a BRUKER AXS (model D8 FOCUS, Germany) using CuKα (λ = 0.154 nm) radiation. The scanning rate and the range were maintained at 1° min^{-1} and $2\theta = 2°$ to 70°.

4.6 Thermogravimetric analysis (TGA)

The thermal properties of CP and CPCD were evaluated using a TG analyser (model TGA-50, Shimadzu, Singapore) at a heating rate of 10 °C min^{-1} up to 600 °C in a nitrogen environment.

4.7 Differential scanning calorimetry (DSC)

The heat flow through the samples was analyzed using a differential scanning calorimeter (DSC-60, Shimadzu) at a heating rate of 10 °C min^{-1} up to 350 °C in a nitrogen atmosphere.

4.8 Scanning electron microscopy (SEM)

The surface morphologies of CUR, CP, HPβCD and CPCD were studied using a scanning electron microscope (JEOL JSM-6390LV, Japan) at an accelerated voltage of 5–10 kV. The samples were mounted on a brass holder and sputtered with platinum for the study.

5 Results and discussion

The % yield of CP and that of CPCD were 82% and 95%, respectively.

5.1 Solubility study

The solubilities of CUR, CP, HPβCD and CPCD in distilled water were checked visibly as well as by optical microscopic images and are shown in Fig. 3(a) and (b). The derivative (CP), HPβCD and CPCD were observed to be more dispersed in solution when compared to CUR. Many CUR particles under associated conditions were found to appear when compared to CP when examined under an optical microscope. Both HPβCD and CPCD form a clear solution compared to that of CP. The changes in solubility due to the formation of a derivative or a complex were also checked by UV-Vis spectroscopy. The position of the absorbance peak of CP was found to shift from 430 nm (CUR) to 336 nm. Moreover, the intensity of the peak was more in CP, suggesting an improvement in solubility (Fig. 3c). A similar observation was reported by Sibalan *et al.*[24] This might be due to the alteration of the CUR structure.[25] The intensity of the absorbance peak was highest for CPCD compared to those of CUR and CP, indicating a further enhancement in solubility due to complex formation.[26]

5.2 FTIR study

FTIR spectroscopy was used to determine the synthesis of CP as well as the formation of the inclusion complex of CP with HPβCD. The FTIR spectra of CUR, CP, HPβCD and CPCD are represented in Fig. 4. The FTIR spectrum of CUR displayed a sharp and a small absorption peak at 3509 cm^{-1} and around 3300 cm^{-1} ascribed to the phenolic O–H stretching vibration. Besides, the sharp absorption peaks at 1628 cm^{-1} (mixture of C═C and C═O vibration), 1603 cm^{-1} (stretching vibration of the aromatic ring of CUR), 1509 cm^{-1} (C═O vibration), 1428 cm^{-1} (olefinic C–H bending vibration), 1280 cm^{-1} (aromatic C–O stretching vibrations), 1026/856 cm^{-1} (C–O–C stretching vibration of CUR), 962 cm^{-1} (benzoate *trans* CH vibration) and 728 cm^{-1} (*cis* CH vibration of the aromatic ring) were also obtained for CUR.[27] In the spectrum of CP, many characteristic changes can be visualized compared to CUR. The intense broad peak at 3401 cm^{-1} might be due to the overlap of C–OH and C–NH bond vibration. The multiple peaks at around 2928 cm^{-1} (CH aliphatic), 1594 cm^{-1}, 1718 cm^{-1} (C═N), 1513 cm^{-1}, 1463 cm^{-1}, 1428 cm^{-1} (C═C), 1373 cm^{-1} (C–N), 1276 cm^{-1} (C–O phenolic), 1156 cm^{-1}, and 1030 cm^{-1} (C–O–C) were also noticed for CP.[28] The intense broad characteristic peak of cyclodextrin at 3400 cm^{-1} was due to OH stretching vibration. The intense peaks at 2925 cm^{-1} (C–H assym/sym stretching), 1629 cm^{-1} (H–O–H deformation and of H_2O), 1155 cm^{-1} (C–O–C vibration), 1082 cm^{-1} (C–H, C–O stretching vibration) and 1300–700 cm^{-1} (skeletal C–C vibration) were also observed.[29] In the spectrum of the prepared complex, all the characteristics

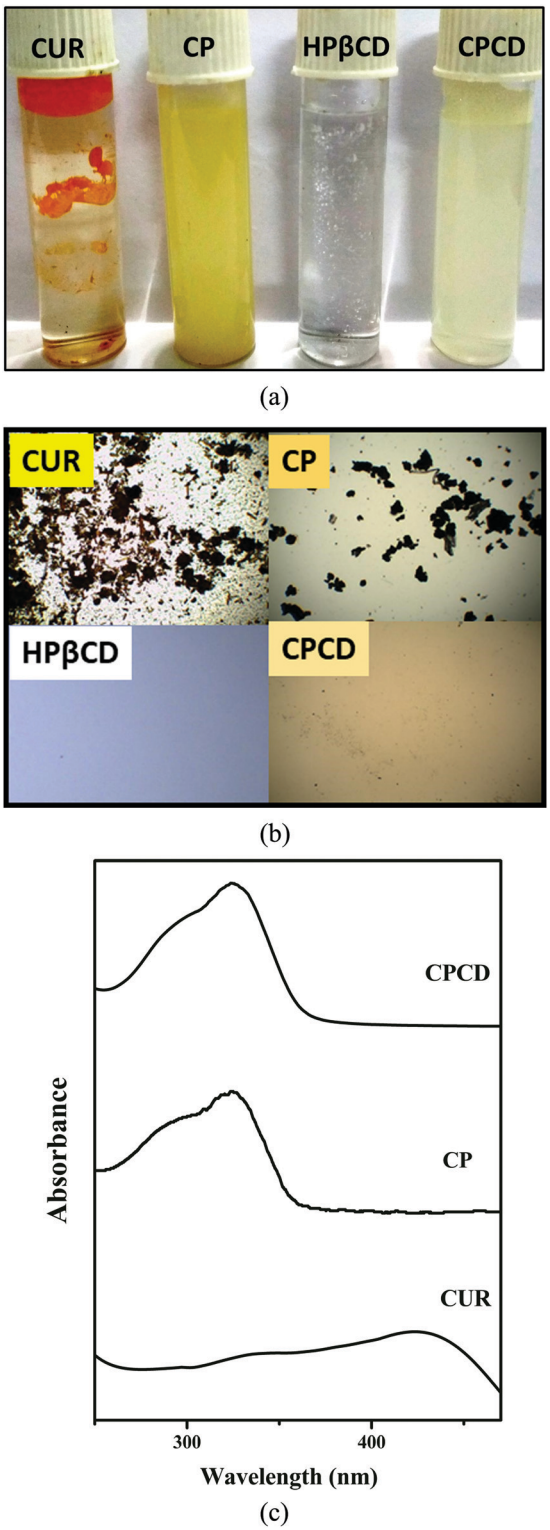

Fig. 3 Aqueous solubility of CUR, CP, HPβCD and CPCD. (a) Visual photographic images. (b) Optical microscopic images and (c) UV-Vis spectra.

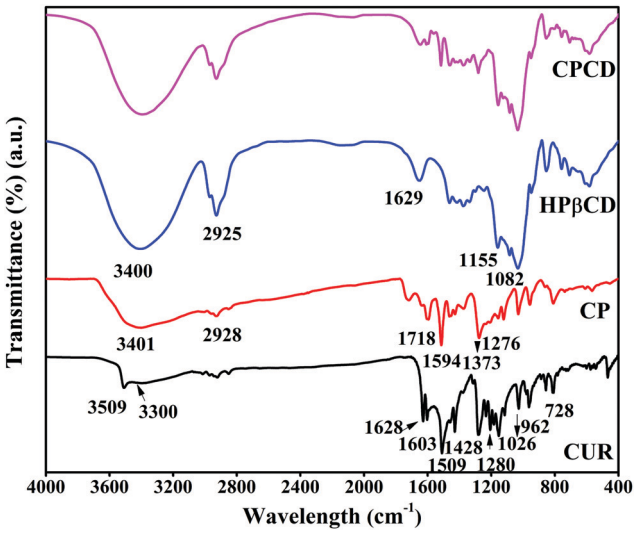

Fig. 4 FTIR spectra of CUR, CP, HPβCD and CPCD.

peaks for HPβCD and CP were noticed, indicating the presence of CP in the CPCD complex.

5.3 NMR study

The synthesis of CP and the formation of CPCD were further confirmed by proton NMR spectroscopy (DMSO-d_6), as shown in Fig. 5. The characteristic peaks for CUR were observed at δ 3.80 (s, 6H, 2 × OCH_3); δ 6.02 (s, 1H, C(O)–CH–C(OH)); δ 6.75 (d, J = 15.6, 2H, 2 × CH = CH–C(O)); δ 6.79 (d, J = 8.2, 2H, 2 × HO–C_q–CH–CH–C_q); and δ 9.03 (s, 2H, 2 × phenolic OH)[30] and those for CP were noticed at δ 6.57 (s, 1H, C(N)–CH–C(NH)); δ 6.73 (d, 2H, 2 × CH═CH–C(O)); δ 6.88–6.90 (m, 4H, 2 × HO–C_q–CH–CH–C_q); δ 7.00 (d, 2H, 2 × CH═CH–C(N)), δ 7.10 (s, 2H, 2 × H_3C–O–C_q–CH–C_q), δ 3.79 (s, 6H, 2 × OCH_3), δ 9.11 (s, 2H, 2 × OH) and δ 12.70 (s, 1H, enolic OH).[11] HPβCD represented in Fig. 1 shows characteristic peaks in the ranges of δ 3.85–4.10 (H3 and H8), δ 3.5–3.75 (H2, H4 and H7) and δ 3.70–3.85 (H5 and H6).[31] In the spectrum of the prepared complex, both the characteristic peaks of HPβCD and CP were observed with some changes in the peak position and intensity. The signals in the range δ 6.58–7.10 were due to the aromatic protons of the pyrazole derivative. The broad peaks at δ 3.19–3.79 were due to H1–H8 of HPβCD and the intense signal at δ 3.79 was due to the methoxy group of the derivative. The intense peaks at δ 3.3 and 2.46 (intense) were due to DMSO.

5.4 XRD pattern analysis

Fig. 6 compares the simulated pattern of curcumin (CURS), the experimental pattern of CUR used in the experiment and that of the prepared CP. Fig. 7 displays the XRD pattern of CP, HPβCD and the final prepared complex (CPCD). It was observed that the XRD pattern of CUR seemed to be coalesced compared to the simulated pattern due to instrumentation. The space group was found to be $P2/n$, and the lattice parameters were as follows: a = 12.70874, b = 7.17209, c = 19.80309 and $\alpha = \gamma = 90^\circ$, $\beta = 95.27^\circ$.[32] Nevertheless, the XRD pattern of CP demonstrates a totally different structure depicting various changes in 2θ values compared to the CUR structure. Some of the significant changes such as the disappearance of some intense peaks at 2θ = 8.99°, 14.57°, 21.30°, and 23.30° and the occurrence of some new peaks at 2θ = 8.49°, 12.68°, 16.92°, 18.37°, 22.34°, and 26.65° along with the enhancement of intensity of some peaks manifested structural changes. Moreover, the XRD pattern of HPβCD was found to be amorphous in nature as revealed by the appearance of a broad peak at around 2θ = 14°.[33] Further, in the diffractogram of the prepared complex, CPCD, the intensity of the peak appeared at 2θ = 18°, suggesting its amorphous nature. Besides, the characteristic crystalline peaks of CP vanished in the

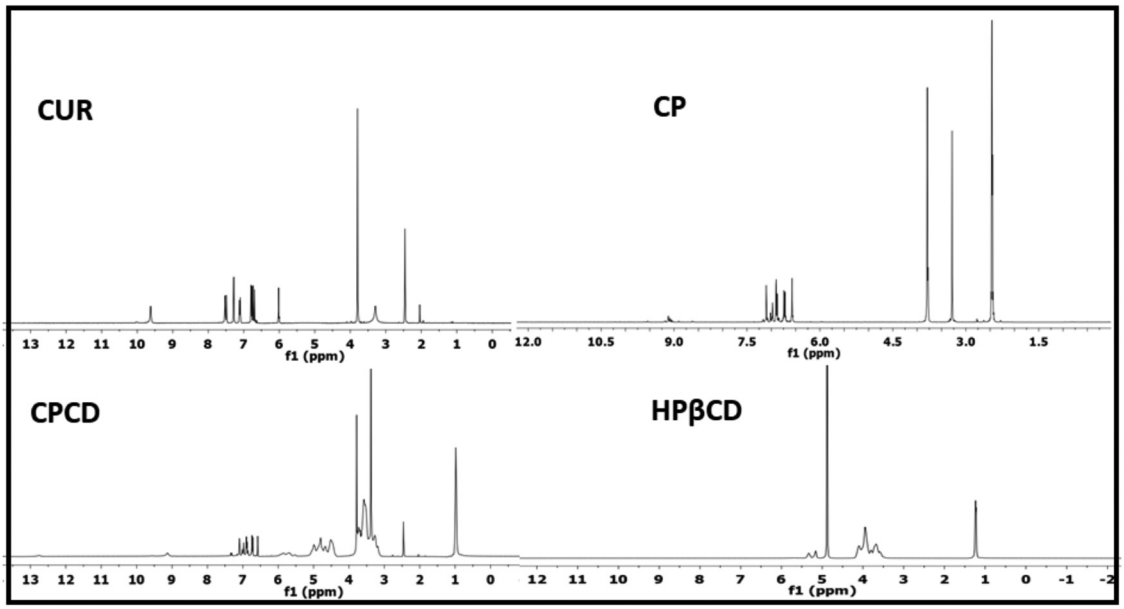

Fig. 5 NMR spectra of CUR, CP, HPβCD and CPCD.

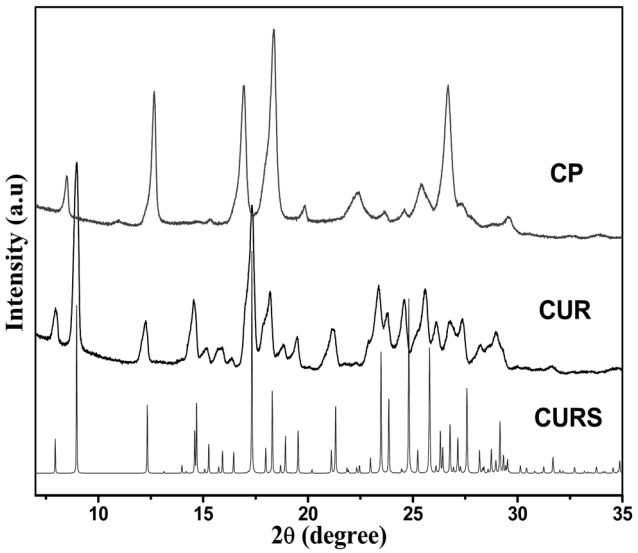

Fig. 6 XRD patterns of CURS, CUR and CP.

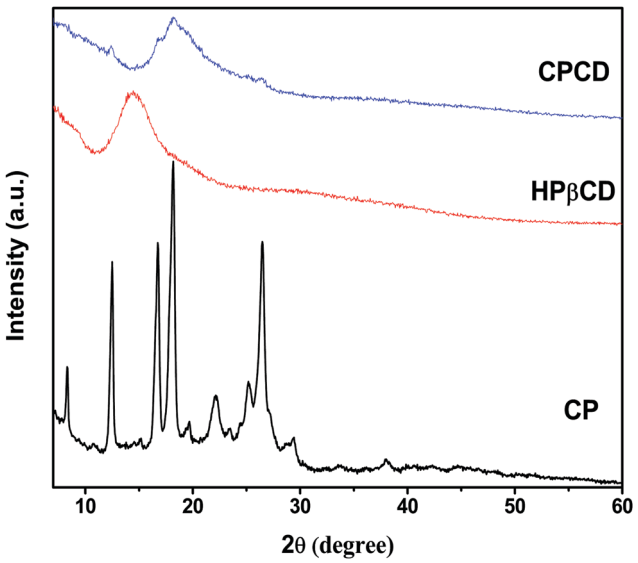

Fig. 7 XRD patterns of CP, HPβCD and CPCD.

XRD pattern of the complex, indicating the successful preparation of the complex.[34]

5.5 TG analysis

The TGA results of CUR, CP, HPβCD and CPCD are summarized in Table 1. In the table, it is clear that the onset of degradation

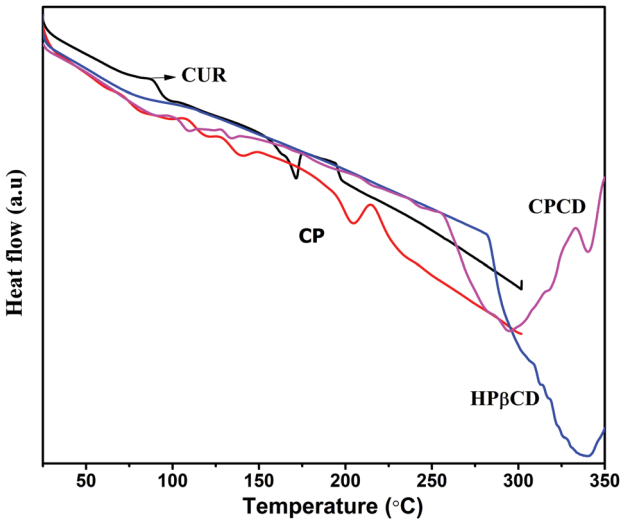

Fig. 8 DSC thermograms of CUR, CP, HPβCD and CPCD.

occurred at 294 °C and 343 °C for CUR and CP, respectively. The onset temperatures of HPβCD and CPCD were in between those of CUR and CP. The maximum peak decomposition temperature was 36 °C for CP and 333 °C for CUR. The maximum peak decomposition temperatures for HPβCD and CPCD were less than that of CP. The T_D values for CP were higher than those of CUR and CPCD. From the table, it can be concluded that the synthesized derivative (CP) showed a better thermal activity than CUR. Similarly, the complex (CPCD) formed by CP and HPβCD exhibited a better thermal stability than HPβCD, which might be due to the enhancement in interaction between the components either chemically or physically during the formation of the derivative (CP) or inclusion complex (CPCD).[26]

5.6 DSC analysis

The DSC thermograms of CUR, CP, HPβCD and CPCD are shown in Fig. 8. CUR and CP showed endothermic peaks at 171 °C and 187 °C, indicating the improvement in the melting point of CP. The endothermic peak that appeared at 337 °C was the melting point of HPβCD. In the case of CPCD, the peak corresponding to CP at 187 °C was found to disappear and the melting peak at 337 °C belonging to HPβCD shifted to 295 °C. This suggested the formation of the complex between CP and HPβCD.[35]

5.7 SEM analysis

Although SEM analysis is not confirmative for the formation of an inclusion complex, the morphology of the samples can

Table 1 Thermogravimetric analysis of CUR, CP, HPβCD and CPCD

Sample name	Onset temperature (°C)	End set temperature (°C)	Maximum decomposition temperature (°C)	Temperature of decomposition (T_D) at different weight loss (%) (°C)			Residue (%) at 600 °C
				20%	35%	60%	
CUR	294	393	333	314	359	510	32
CP	343	397	369	375	443	—	57
HPβCD	332	369	351	328	344	355	5
CPCD	341	372	352	335	348	366	17

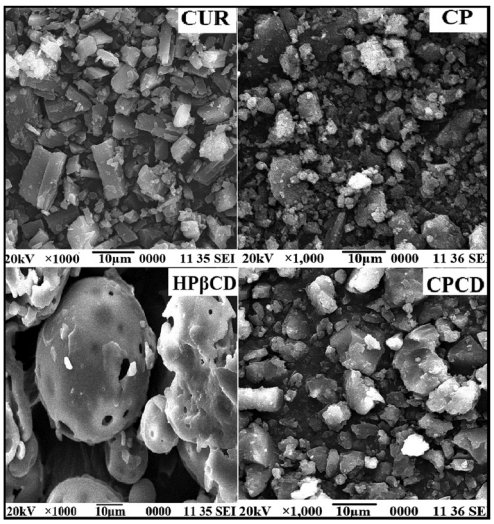

Fig. 9 SEM images of CUR, CP, HPβCD and CPCD.

be visualized. The microphotographs of CUR, CP, HPβCD and CPCD are portrayed in Fig. 9. It was observed that CUR showed a somewhat irregular and rod-shaped structure and CP displayed a granular-like structure, indicating a change in morphological features due to synthesization. HPβCD exhibited a spherical structure with some pores on the surface. The morphological features of the inclusion complex, CPCD, were neither a granular form nor a spherical form. This change in surface features might be due to the formation of a new solid structure of the complex. A combination of the morphology of DEN and HPβCD was reported by Ashwaq *et al.* while studying the morphology of the DEN-HPβCD complex by FESEM.[36]

5.8 Swelling study

An important governing factor for drug release behavior from a complex is the swelling nature of the polymer, which depends on its nature, size and surface morphology. Reports on the effect of structure on the swelling behavior of samples can be found in the literature.[37,38] The hydrophilic nature and porous surface of HPβCD are some of the causes for its swelling and drug release behaviour. The swelling behavior of the prepared complex (CPCD) was checked at two different pH values (7.4 and 1.2) mimicking intestinal and gastric pH conditions. From the swelling (%) *vs.* time plot shown in Fig. 10(a), it was noticed that at pH 7.4, there was an initial abrupt swelling and then it levelled off. The swelling (%) was almost 198% at the end of 24 h. In the case of pH 1.2, swelling of the complex increased initially but not so rapidly as that of the complex at pH 7.4 and after that, it remained almost constant throughout the time period studied. It was also observed that the percentage of swelling was more in the alkaline medium than in the acidic medium. This might be due to the increase in the ionization of hydroxyl groups at a higher pH, resulting in an increase in swelling (%).[39]

5.9 *In vitro* release study

The cumulative release behavior of the drug from the complex depends on the swelling behavior of the polymer and the solubility of the drug in the release medium.[40] The cumulative release pattern with respect to time is portrayed in Fig. 10(b). The release behavior of the drug was found to follow a similar pattern to that of the results observed in the swelling study. The cumulative release (%) of the drug in both acidic and basic media was rapid initially and then slowed with the increase of time. In acidic medium, HPβCD swelled less and hence the drug release was found to be less. At a higher pH, the polymer HPβCD swelled more and hence the drug release was high.[41] The amorphous nature of the complex (as judged by the XRD study) might also be a reason for the higher release.[42]

6 Toxicity study

During systemic drug delivery, the samples might cause impairment in human lymphocyte cells. Hence, for the sake of biosafety,

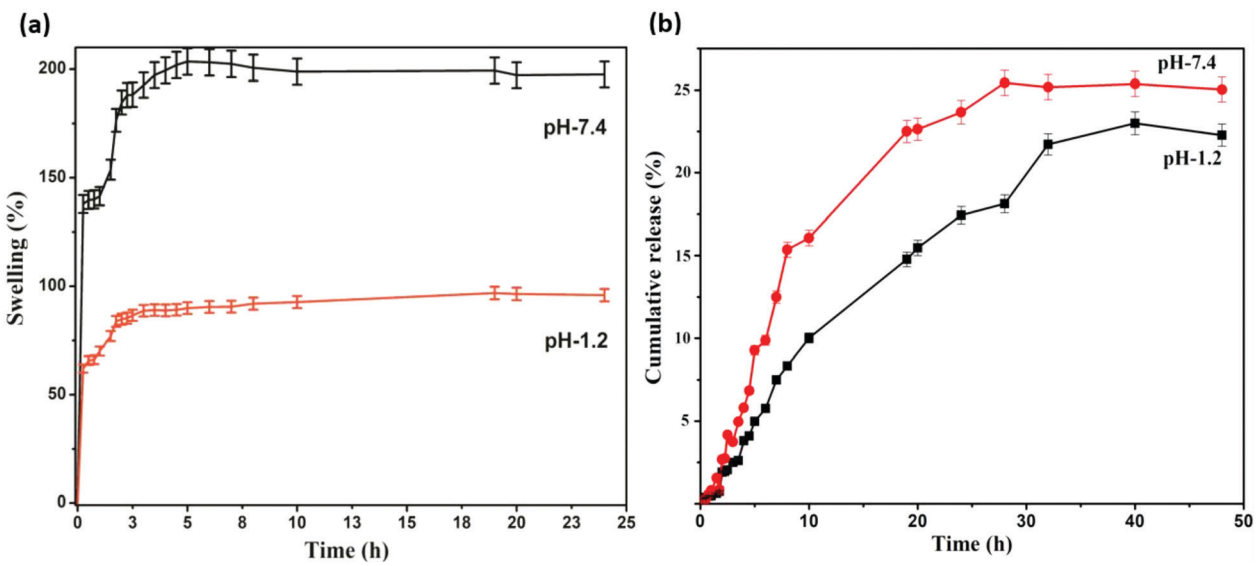

Fig. 10 (a) Swelling degree of CPCD under acidic and basic pH conditions for 24 h. (b) Cumulative release behaviour of CP from CPCD under both acidic and basic pH conditions for 48 h.

the samples were investigated for their biocompatibility in human lymphocytic cells and cancer cell lines.

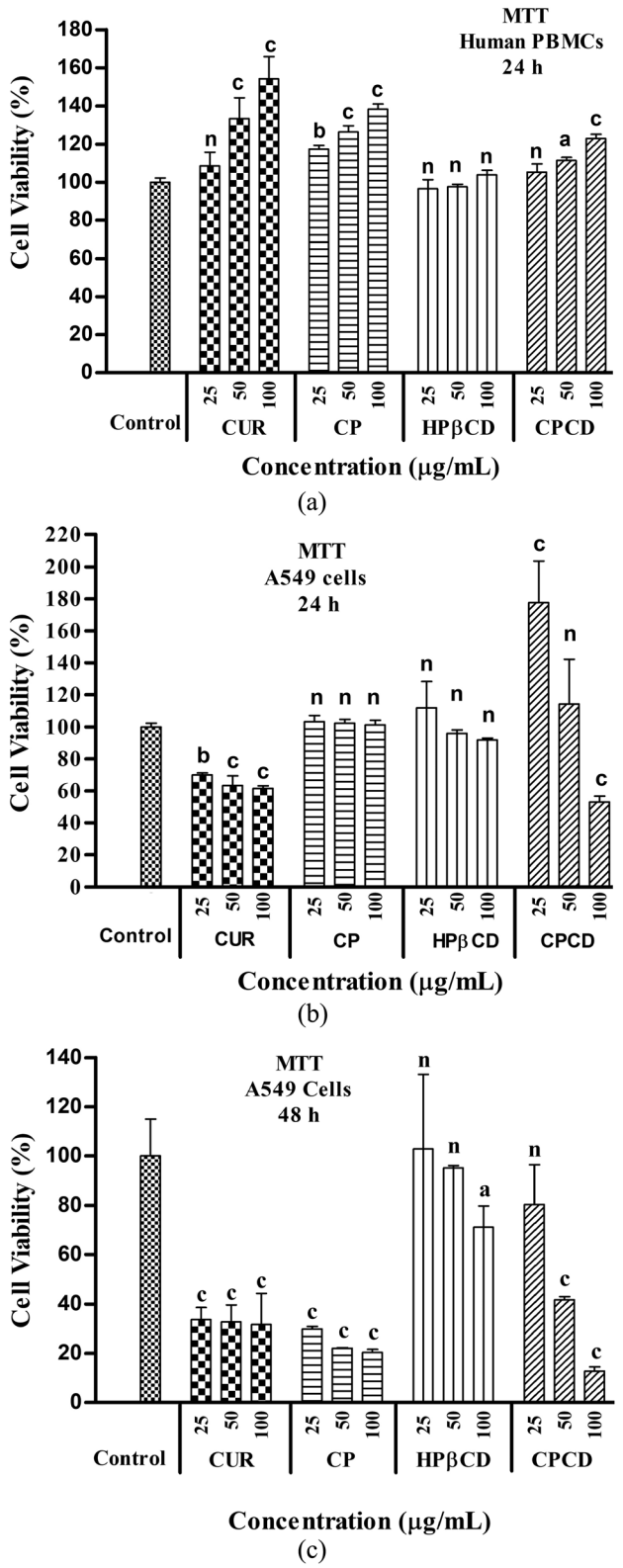

Fig. 11 Effect of CUR, CP, HPβCD and CPCD with increasing doses (25–100 μg mL^{-1}) on the cell viability through MTT assay in (a) human PBMCs at 24 h. (b) A549 cancer cell lines at 24 h and (c) A549 cancer cell lines at 48 h.

6.1 Cell viability in human peripheral blood mononuclear cells (PBMCs)

The biocompatibility of CUR, CP, HPβCD and CPCD was investigated through MTT assay in human lymphocytes for 24 h in the concentration range from 25 to 100 μg mL^{-1}, as shown in Fig. 11(a). In the experiment, 0.1% DMSO was used as the control. It was observed that the cell viability of the CUR-treated cells increased with increasing CUR concentration. The increase in cell viability with the increase in the concentration of CUR was reported in the literature.[43] CP also showed an increase in cell viability but the effect was much less than that of CUR. Similarly, a small increase in cell viability was also observed in the case of CPCD. The reason behind the cell proliferation for both CP and CPCD was not clear. However, the lower cell viability of CPCD compared to that of CP might be due to the slow release of CP from the complex. Furthermore, with the increase in concentration of HPβCD, a marginal increase in cell viability was also observed. It was reported in the literature that a lower concentration of methyl-β-cyclodextrin could enhance the proliferation of lymphocytes in human PBMCs.[44] Overall, the results indicated that all the samples using the aforementioned concentration were non-toxic to human lymphocyte cells.

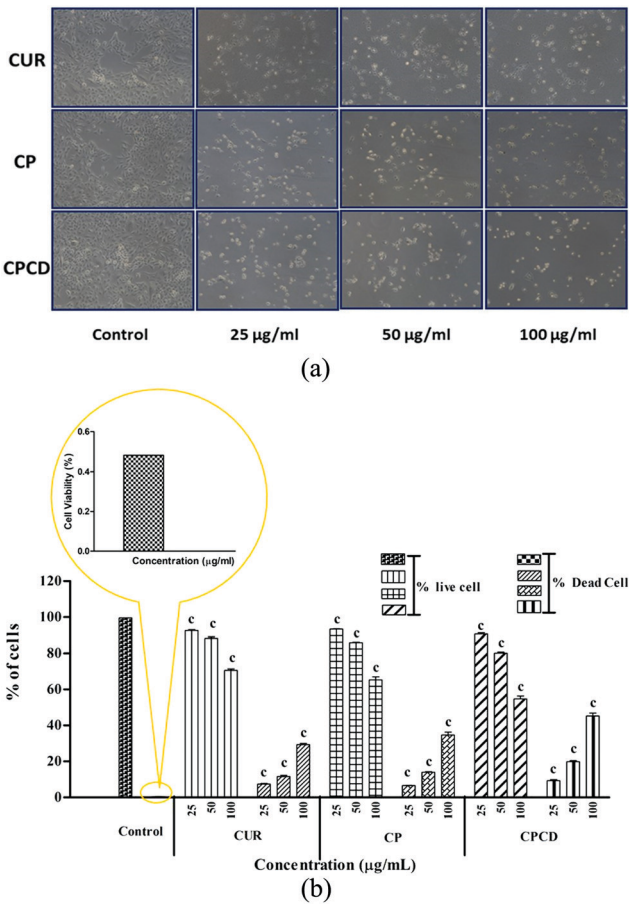

Fig. 12 Effect of CUR, CP and CPCD with increasing doses (25–100 μg mL^{-1}) on cell viability through cell counting in A549 cancer cell lines for 48 h. (a) Microscopic images and (b) graphical representation.

6.2 Cell viability in A549 cancer cell lines

A549 lung cancer cell lines were treated with the samples to check their viability through MTT assay. The cells were treated with different concentrations (25–100 μg mL^{-1}) of samples for 24 h (Fig. 11b) and 48 h (Fig. 11c), respectively. The mentioned figures depict that there is a time-dependent decrease in cell viability in all the samples. However, all the samples treated for 24 h displayed some cytotoxicity except CP. At this time interval, CP showed a negligible amount of cytotoxicity similar to that of human lymphocytes. The reason for this is not clear, as stated earlier. The cytotoxicity of the CP-treated cells at 48 h was higher than that of the CUR-treated cells, but the results were not significant enough. Further, the inclusion complex CPCD showed a higher cytotoxicity against the A549 cancer cells at a higher dose (100 μg mL^{-1}) compared to those of CUR and CP at 48 h. This could be attributed to the higher release of CP from the inclusion complex.

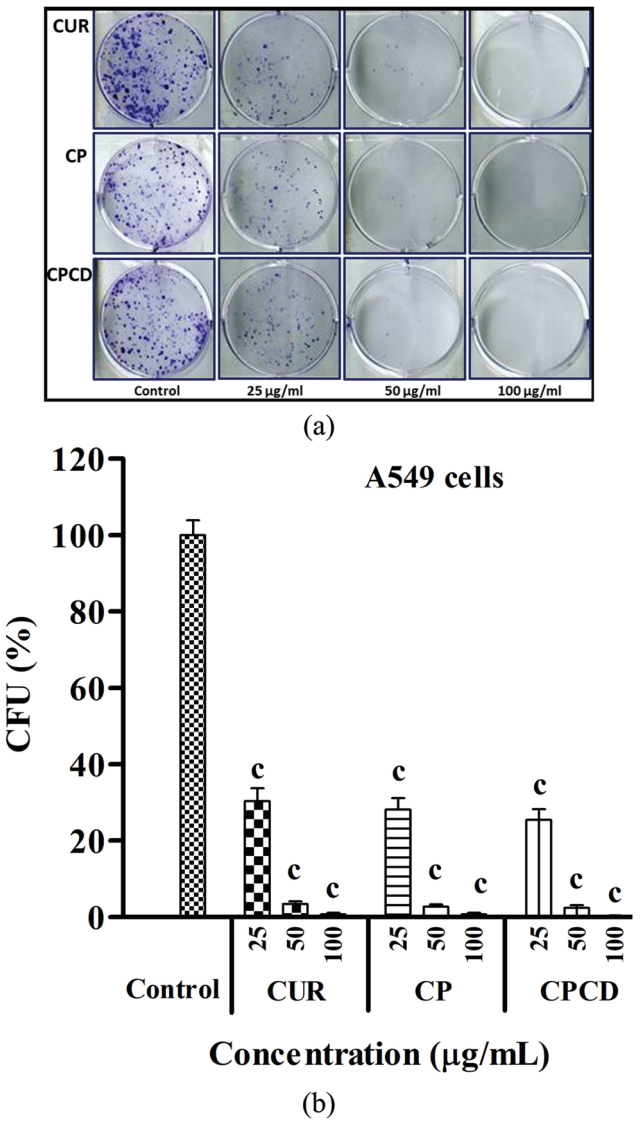

Fig. 13 Effect of CUR, CP and CPCD on A549 cancer cell colonies with increasing doses (25–100 μg mL^{-1}). (a) Photographs and (b) graphical representation.

6.3 Cell viability through cell counting by the trypan blue exclusion method

The cell viability in the A549 lung cancer cell lines was confirmed by cell counting by the trypan blue exclusion method, as shown in Fig. 12. The cell viability (%) decreased in a dose-dependent manner in the concentration range of 25–100 μg mL^{-1} at 48 h. The results suggested that the effect of CPCD was not different compared to those of either CUR or CP in killing the cancer cells.

6.4 Clonogenic assay

Clonogenic assay was performed to evaluate the long-term anticancer efficacy of CUR, CP and CPCD in the A549 lung cancer cell lines. The cells were incubated with equivalent doses (25–100 μg mL^{-1}) of the drugs for 48 h and after that the drugs were washed out, and the cells were kept in fresh media for 10 days. It was observed from the graph (Fig. 13) that the CFU% (colony forming unit) showed a dose-dependent decrease in colony formation in all the three samples. Cells treated with CUR, CP and CPCD showed fewer colonies compared to the control. Although CPCD exhibited a marginal decrease in colony formation compared to CUR and CP, the differences are small. Yallapu *et al.*[26] reported that the CUR–βCD inclusion complex formed fewer colonies compared to free CUR due to the sustained release of CUR from the complex. These results indicated that CP and CPCD showed a cell growth inhibitory effect in the A549 cancer cell lines similar to that of CUR.

7 Conclusion

The curcumin pyrazole derivative was synthesized and its complexation with HPβCD was achieved, as confirmed by FTIR spectroscopy, UV-Vis spectroscopy and NMR spectroscopy. The complexation leads to a significant improvement in physicochemical properties such as solubility and thermal stability. Moreover, the results revealed that the structural modification of curcumin and its further complexation did not change the anticancer activity significantly as judged by MTT assay, cell counting and clonogenic assay. Further, CP did not demonstrate any cytotoxicity towards human PBMCs and cancer cell lines when treated for 24 h. The reasons for this are unknown and need to be investigated further. Therefore, the prepared complex enhanced some of the physical properties without affecting the inherent properties of curcumin.

Consent for experimentation

The authors have the consent from the Tezpur University Ethical Committee (TUEC) for the use of the isolated lymphocytes as a test model.

Conflicts of interest

There are no conflicts to declare.

Acknowledgements

The authors would like to acknowledge Tezpur University for providing the necessary technical facilities and infrastructure to carry out the research work. Also, financial support in the form of a Maulana Azad National Fellowship (MANF) (Award letter no. F117.1/201516/MANF201517ASS67730), UGC, Government of India, is highly acknowledged by Bably Khatun.

Notes and references

1 S. C. Angadi, L. S. Manjeshwar and T. M. Aminabhavi, *Int. J. Biol. Macromol.*, 2010, **47**, 171–179.
2 S. Prylutska, I. Grynyuk, A. Grebinyk, V. Hurmach, I. Shatrava, T. Sliva, V. Amirkhanov, Y. Prylutskyy, O. Matyshevska and M. Slobodyanik, *et al.*, *Nanoscale Res. Lett.*, 2017, **12**, 124.
3 S. Mishra, S. Patel and C. G. Halpani, *Chem. Biodiversity*, 2019, **16**, e1800366.
4 N. Li, N. Wang, T. Wu, C. Qiu, X. Wang, S. Jiang, Z. Zhang, T. Liu, C. Wei and T. Wang, *Drug Dev. Ind. Pharm.*, 2018, **44**, 1966–1974.
5 H. R. Puneeth, H. Ananda, K. S. S. Kumar, K. S. Rangappa and A. C. Sharada, *Med. Chem. Res.*, 2016, **25**, 1842–1851.
6 N. S. Jha, S. Mishra, S. K. Jha and A. Surolia, *Electrochim. Acta*, 2015, **151**, 574–583.
7 V. R. Yadav, S. Suresh, K. Devi and S. Yadav, *AAPS PharmSciTech*, 2009, **10**, 752.
8 K. Kaur, S. Uppal, R. Kaur, J. Agarwal and S. K. Mehta, *New J. Chem.*, 2015, **39**, 8855–8865.
9 A. P. Sherje, V. Kulkarni, M. Murahari, U. Y. Nayak, P. Bhat, V. Suvarna and B. Dravyakar, *Mol. Pharmaceutics*, 2017, **14**, 1231–1242.
10 H. Cetin Babaoglu, A. Bayrak, N. Ozdemir and N. Ozgun, *J. Food Process. Preserv.*, 2017, **41**, e13202.
11 R. Narlawar, M. Pickhardt, S. Leuchtenberger, K. Baumann, S. Krause, T. Dyrks, S. Weggen, E. Mandelkow and B. Schmidt, *ChemMedChem*, 2008, **3**, 165–172.
12 N. Ahsan, S. Mishra, M. K. Jain, A. Surolia and S. Gupta, *Sci. Rep.*, 2015, **5**, 9862.
13 C. Jantarat, P. Sirathanarun, S. Ratanapongsai, P. Watcharakan, S. Sunyapong and A. Wadu, *Trop. J. Pharm. Res.*, 2014, **13**, 1215–1223.
14 N. Banik, M. Iman, A. Hussain, A. Ramteke, R. Boruah and T. K. Maji, *New J. Chem.*, 2013, **37**, 3981–3990.
15 O. M. Paduraru, A. Bosnceanu, G. Tantaru and C. Vasile, *Ind. Eng. Chem. Res.*, 2013, **52**, 2174–2181.
16 N. Banik, A. Hussain, A. Ramteke, H. K. Sharma and T. K. Maji, *RSC Adv.*, 2012, **2**, 10519–10528.
17 C. Saikia, M. K. Das, A. Ramteke and T. K. Maji, *Int. J. Biol. Macromol.*, 2016, **93**, 1121–1132.
18 M. P. Curry, S. Norris, L. Golden-Mason, D. G. Doherty, T. Deignan, C. Collins, O. Traynor, G. P. McEntee, J. E. Hegarty and C. O'Farrelly, *J. Immunol. Methods*, 2000, **242**, 21–31.
19 M. Gómez-Lechón, F. Iborra, I. Azorn, C. Guerri and J. Renau-Piqueras, *J. Tissue Cult. Methods*, 1992, **14**, 73–77.
20 F. Denizot and R. Lang, *J. Immunol. Methods*, 1986, **89**, 271–277.
21 J.-W. Lee, F. Serna, J. Nickels and C. E. Schmidt, *Biomacromolecules*, 2006, **7**, 1692–1695.
22 Y. Sun, M. Zou, C. Hu, Y. Qin, X. Song, N. Lu and Q. Guo, *Food Chem. Toxicol.*, 2013, **51**, 53–60.
23 S. J. Koppikar, A. S. Choudhari, S. A. Suryavanshi, S. Kumari, S. Chattopadhyay and R. Kaul-Ghanekar, *BMC Cancer*, 2010, **10**, 210.
24 R. Sribalan, G. Shakambari, G. Banuppriya, P. Varalakshmi, E. R. Subramanian, S. Sudhakar and V. Padmini, *ChemistrySelect*, 2017, **2**, 1122–1128.
25 J. Yu and A. Kudo, *Adv. Funct. Mater.*, 2006, **16**, 2163–2169.
26 M. M. Yallapu, M. Jaggi and S. C. Chauhan, *Colloids Surf., B*, 2010, **79**, 113–125.
27 P. K. Mohan, G. Sreelakshmi, C. Muraleedharan and R. Joseph, *Vib. Spectrosc.*, 2012, **62**, 77–84.
28 O. A. Hamed, N. Mehdawi, A. A. Taha, E. M. Hamed, M. A. Al-Nuri and A. S. Hussein, *Iran. J. Pharm. Res.*, 2013, **12**, 47.
29 Y. Yao, Y. Xie, C. Hong, G. Li, H. Shen and G. Ji, *Carbohydr. Polym.*, 2014, **110**, 329–337.
30 C. A. Slabber, C. D. Grimmer and R. S. Robinson, *J. Nat. Prod.*, 2016, **79**, 2726–2730.
31 C.-M. Hsu, S.-C. Yu, F.-J. Tsai and Y. Tsai, *Carbohydr. Polym.*, 2013, **98**, 1422–1429.
32 P. Sanphui, N. R. Goud, U. R. Khandavilli, S. Bhanoth and A. Nangia, *Chem. Commun.*, 2011, **47**, 5013–5015.
33 J. Chen, X. Qin, S. Zhong, S. Chen, W. Su and Y. Liu, *Molecules*, 2018, **23**, 1179.
34 C. S. Mangolim, C. Moriwaki, A. C. Nogueira, F. Sato, M. L. Baesso, A. M. Neto and G. Matioli, *Food Chem.*, 2014, **153**, 361–370.
35 A. Anitha, M. Murugan and R. Rajamohan, *Spectrosc. Lett.*, 2018, **51**, 198–204.
36 A.-A. S. Ashwaq, A. Rasedee, A. B. Abdul, Y. H. Taufiq-Yap, M. S. Al-Qubaisi and E. E. Eid, *J. Inclusion Phenom. Macrocyclic Chem.*, 2017, **87**, 167–178.
37 L. B. Sukhodub, L. F. Sukhodub, Y. I. Prylutskyy, N. Y. Strutynska, L. Vovchenko, V. Soroca, N. Slobodyanik, N. Tsierkezos and U. Ritter, *Mater. Sci. Eng., C*, 2018, **93**, 606–614.
38 L. Sukhodub, L. Sukhodub, M. Kumeda, S. Prylutska, V. Deineka, Y. I. Prylutskyy and U. Ritter, *Carbohydr. Polym.*, 2019, **223**, 115067.
39 A. Hedges, *Starch*, Elsevier, 2009, pp. 833–851.
40 S. S. Patil, H. Doddayya, V. Gupta and K. Gupta, *Int. J. Pharm. Pharm. Sci.*, 2014, **6**, 324–327.
41 S. Baboota, M. Dhaliwal and K. Kohli, *AAPS PharmSciTech*, 2005, **6**, E83–E90.
42 B. Khatun, N. Banik, A. Hussain, A. Ramteke and T. Maji, *J. Microencapsulation*, 2018, **35**, 439–453.
43 J.-H. Kim, S.-H. Park, S.-W. Nam, H.-J. Kwon, B.-W. Kim, W.-J. Kim and Y. H. Choi, *Int. J. Mol. Med.*, 2011, **28**, 429–435.
44 H.-Z. Lü, A.-Y. Zhu, Y. Chen, J. Tang and B.-Q. Li, *Hum. Immunol.*, 2011, **72**, 538–546.